JCTC Journal of Chemical Theory and Computation

First Hybrid Embedding Scheme for Polar Covalent Materials Using an Extended Border Region To Minimize Boundary Effects on the Quantum Region

Alexei M. Shor,[†] Elena A. Ivanova Shor,[†] Vladimir A. Nasluzov,*[,†] Georgi N. Vayssilov,[‡] and Notker Rösch*[,§]

Institute of Chemistry and Chemical Technology, Russian Academy of Sciences, 660049 Krasnoyarsk, Russian Federation, Faculty of Chemistry, University of Sofia, 1126 Sofia, Bulgaria, and Department Chemie, Technische Universität München, 85747 Garching, Germany

Received June 27, 2007

Abstract: We present an improved scheme for constructing the border region within a hybrid quantum mechanics/molecular mechanics (QM/MM) embedded cluster approach for zeolites and covalent oxides that ensures proper modeling of adsorption complexes with QM regions of moderate size. The procedure employs a flexible orbital basis set on monovalent oxygen pseudoatoms at the boundary of the QM cluster and introduces a pseudopotential description without explicit representation of valence electrons for their immediate Si neighbors in the MM region. This novel QM/MM border scheme, implemented in the elastic polarizable environment method for polar covalent materials (covEPE), provides an accurate description of the local structure of zeolites and other silica based materials. We assessed the performance of the novel border scheme by comparing calculated and experimental results for structures, vibrational frequencies, and binding energies of CO adsorption complexes at bridging OH groups in zeolites with FAU and MFI structures. In addition, when modeling zeolite-supported metal clusters, the new approach implies considerably reduced corrections due to the basis set superposition error, compared to our previous scheme for treating the border region of the QM partition [*J. Phys. Chem. B* **2003**, *107*, 2228].

1. Introduction

One of the most crucial features of a reliable hybrid quantum mechanics/molecular mechanics (QM/MM) scheme is an adequate construction of the border region between two subsystems.[1] With specific chemical bonding situations in mind, various schemes have been proposed to construct the border region between QM and MM partitions of a system.[2] In strongly ionic oxides such as MgO, the system can be partitioned into QM and MM regions without the QM/MM boundary cutting covalent bonds; in addition, atomic (ionic) centers at the border of the QM part are the same as inside the QM cluster. A characteristic challenge of QM/MM schemes for such systems is an artificial polarization of anionic centers at the border of the QM cluster due to neighboring cations of the MM region as the latter type of centers is represented by positive point charges. This artifact can be avoided by augmenting the representation of cations in the MM region immediately at the QM/MM boundary by total ion model potentials (TIMPs) which provide the proper repulsive contributions to electrons of anionic centers in the vicinity.[3] Hybrid schemes for systems with covalent bonding require a more complicated description of the border region because any partitioning of the system into QM and MM parts will cut covalent bonds. Various strategies have been

* Corresponding author e-mail: nv@icct.ru (V.A.N.), roesch@ch.tum.de (N.R.).
[†] Russian Academy of Sciences.
[‡] University of Sofia.
[§] Technische Universität München.

10.1021/ct700159k CCC: $37.00
Published on Web 10/17/2007

proposed to handle the resulting "dangling" bonds of the QM cluster; they are either saturated by hydrogen-like, artificial "link" atoms located between two centers on either side of the QM/MM boundary[1,4] or by invoking a special description for centers at the border of the QM region that compensates for the missing covalently bonded partner.[5]

Covalently bonded materials with some polar interactions are among the most complex systems for such modeling because both types of complications just mentioned can be encountered in a QM/MM scheme. For materials of this type, e.g., zeolites, we recently proposed the hybrid density functional/molecular mechanics (DF/MM) embedded cluster method covEPE.[6,7] In a preceding study[6] we described features and intrinsic problems of different types of cluster embedding schemes developed for modeling of zeolites[1,2,4] and silica.[8] Recently, those methods were applied to various problems, e.g., structural defects[9] and catalytic reactions.[10] A related new methodological development is the extension of the QM-pot scheme,[11] based on an "energy-subtraction" scheme; it combines periodic DF calculations as a low-level method with MP2 calculations of an embedded cluster model as a high-level method.

A key feature of our covEPE embedding scheme[6,7] is the representation of the oxygen centers at the border of the QM cluster by a specially parametrized pseudopotential O* which renders these species monovalent. To ensure consistency between the treatment of the QM and MM parts of the system, we developed a specific force field, parametrized on the basis of DF calculations. We found this approach suitable for modeling electronic and geometrical properties of isolated active sites of various zeolites (CHA, FAU, MFI), including pure silicalite as well as zeolites doped with Al and Ti atoms at framework positions.[6−12]

In that first covEPE parametrization we followed an earlier suggestion[6] and constructed the pseudopotentials for boundary centers with the rather small basis set (2s2p) for computational efficiency. As a consequence, one should avoid QM cluster models where this relatively poor representation of O* centers directly affects the description of the active center. Relatively close contacts with a larger adsorbate may induce an artificial interaction due to the fact that atoms in the QM region close to O* centers are usually described by very flexible basis sets, e.g., adsorbed transition metal species. As a result of the unbalanced description, one may encounter an artificial attraction between the adsorbate and border centers O*. Such artifacts are easily discernible via large counterpoise corrections when one estimates the basis set superposition error (BSSE) of the adsorption energy; below we will discuss this in more detail.

Unfortunately, the peculiar three-dimensional structure of zeolite frameworks renders it difficult to avoid such artificial interactions unless one opts for rather large QM models which, in turn, reduce the benefit of a hybrid QM/MM approach. In the present work, we opted for an alternative which relies on an improved, more flexible description of the pseudoatoms O*. In this augmented approach, the two-dimensional surface through the O* centers, which originally partitioned space into QM and MM regions, is extended to a formally three-dimensional boundary region which, besides

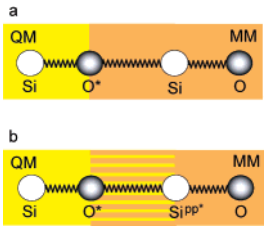

Figure 1. Structure of the border QM/MM region in the (a) previous and (b) the proposed novel extended termination scheme.

the O* pseudoatoms of the QM cluster, also includes their immediate cationic neighbors in the MM region, Si^{PP}*, in the form of total ion model potentials (TIMPs). This choice formally combines the two previous variants of the EPE scheme;[3,6] it was motivated by the need to avoid (or, at least, to reduce strongly) the otherwise significant and unwanted polarization of O* centers. Hence, this improved covEPE method, to be presented here, is based on an *extended boundary region*.

In the following, we will first discuss in detail the parametrization strategy for the new border centers O* and Si^{PP}*. Then we will evaluate the new variant of the covEPE embedding scheme by calculating (i) structural and spectral characteristics of two zeolite models, silicalite and Al-containing structures, based on a faujasite lattice as well as (ii) adsorption complexes of CO probe molecules and hexarhodium clusters in zeolite cavities.

2. The Novel covEPE Parametrization

2.1. Representation of the Border Region. A defining feature of the new covEPE parametrization is the representation of the border between the QM and MM partitions by pairs of atoms O*(QM)−Si^{PP}*(MM) that form a covalent bond of the original material (Figure 1). As in the original covEPE method, the charge of the whole QM/MM system is balanced by assigning incremental point charge Δq_{pp} to O* border pseudoatoms; these increments are half of the charge of oxygen centers in the MM region. As before, there are no dangling bonds at the QM boundary, because the O* centers are represented by adjusted pseudopotentials, carrying seven valence electrons, which renders these "pseudo"-oxygen centers monovalent. In the present implementation, we chose to describe O* centers with semilocal effective core potentials of the Stuttgart type:[13]

$$V(r) = -\frac{Q}{r} + \sum_l \sum_k A_{kl} \exp(-a_{kl} r^2) \sum_{m_l} |lm_l\rangle\langle lm_l| \quad (1)$$

Here, Q is the charge of the ionic core, while l and m_l are quantum numbers that designate eigenfunctions $|lm_l\rangle$ of the orbital angular momentum. The ten parameters of this pseudopotential were adjusted by starting with those of fluorine.[14] The previous implementation was based on a SBK pseudopotential[15] which (for fluorine) features only six adjustable parameters, hence it is less flexible. The valence orbital basis set of O* was derived from a (9s5p1d) all-electron basis set of F by removing the four largest s exponents.[16] The exponents of the resulting (5s5p1d) basis

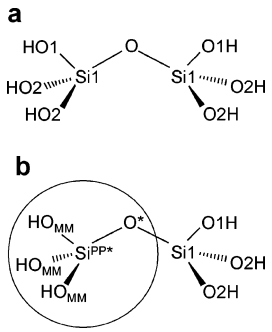

Figure 2. Sketch of systems used for fitting the pseudopotential parameters: (a) reference system calculated at the QM level and (b) target hybrid QM/MM system.

set were then adjusted as described below. This new basis set of O*, contracted to [4s3p1d], is considerably more flexible than the contracted [2s2p] basis set used previously with the SBK pseudopotential.[6] The new basis is of the same quality as the basis sets used for adsorbates and centers inside the QM region of the zeolite; therefore, counterpoise corrections of adsorption energies are significantly smaller (see sections 4.3 and 4.4).

However, neighboring bare positive point charges that represent Si cations of the MM region result in an artificial polarization of the new O* centers due to their flexible basis set. This problem is well-known from embedded cluster models of strongly ionic oxides.[3] To ensure an adequate polarization of O* centers, we followed the same strategy as in the EPE approach of ionic oxides:[3] we assigned a repulsive Si^{PP}* TIMPs (without any orbital basis set) to those cationic Si centers of the MM part that are located immediately at the QM/MM interface. Consistent with the O* pseudopotential, we chose to represent Si^{PP}* centers also by pseudopotentials of Stuttgart type. Parameter adjustment of Si^{PP}* centers was started with the values of sodium.[17] For Si^{PP}* centers at the QM/MM border we assumed the same effective charge, 1.2 *e*, as for their MM analogues of our silicate force field (FF) of shell-model type with potential derived charges (PDCs).[6,7]

2.2. Procedure of the Parametrization. We determined the parameters of O* and Si^{PP}* pseudoatoms in an iterative two-step procedure, similar to the strategy we used to establish the original covEPE scheme.[6] Some modifications were required because the new description of the QM/MM border is more sophisticated. In the first step of each iteration, we optimized the exponents of the O* basis set by minimizing the energy of an isolated pseudoatom O* that carries an incremental charge $\Delta q_{pp} = -0.3\ e$; that increment is derived from the potential derived charge, $-0.6\ e$, of oxygen centers in the MM region.[6] In a second step, the pseudopotential parameters of both types of border atoms, O* and Si^{PP}*, were adjusted to reproduce (i) selected electronic and structural characteristics of an isolated cluster which represents part of a zeolite framework and (ii) the electrostatic potential (ESP) produced by a periodic zeolite framework.

The reference data of type (i) had been produced by calculating the 2T model cluster $(HO)_3SiOSi(OH)_3$ at the QM level (Figure 2a). In the system to be trained, the $O-Si(OH)_3$ fragment of the reference cluster was replaced by O* and Si^{PP}* centers, and the remaining three OH groups were represented as point charges, $-0.7\ e$ for oxygen and $0.4\ e$ for hydrogen atoms (Figure 2b). These atomic charges for O and H reproduce best the electrostatic potential of the (finite) reference system. As before,[6] we derived the reference data of type (ii) with a periodic array of point charges located at crystallographic positions of a chabazite lattice which contains only Si atoms in tetrahedral positions (T-atoms). To mimic the electrostatic field of this zeolite, we used the same PDCs, $1.2\ e$ for Si and $-0.6\ e$ for O, as reported earlier.[6] The system to be trained was constructed as the cluster $(Si^{PP}*O*)_3SiOSi(O*Si^{PP}*)_3$, embedded in a finite array of point charges which accurately mimics the periodic electrostatic potential of an extended chabazite environment.[3,6]

Using a least-squares approach and the simplex method,[18] we simultaneously optimized the pseudopotential parameters of O* and Si^{PP}*. The training set contained nine types of data, eight of which were derived from the 2T QM cluster: (i−iii) potential energy curves of the bonds Si1−O* and Si1−O1 and the bond angle O*−Si1−O1, each represented by a set of five points; (iv−vii) PDCs of the atoms Si1, O1, O2 and of the oxygen atom that was replaced by an O* pseudoatom; and (viii) the HOMO−LUMO gap.

Contribution (ix) to the least-squares sum was constructed from the ESP of the periodic array of point charges which was probed on a planar grid of 300 points near the center of the 8T ring of chabazite, covering an area of 1.5 Å × 2.0 Å.

After initial tests, the weighting factors of each squared deviation of data (i)−(iii) (in au) were set to 3, those of data (iv)−(viii) (in e and au, respectively) were kept at 1, while those of type (ix) (in au) were set to 0.025.

The potential energy curves calculated for the reference 2T cluster and the "trained" system with the final parameters for the O* and Si^{PP}* border atoms are provided as Supporting Information (Figure S1, Tables S1 and S2). The O*−Si1−O1 bending potential energy curves calculated for the pure QM reference cluster and the trained hybrid QM/MM system agree very well. The Si1−O* and Si1−O1 energy show some deviations, but the discrepancy never exceeds 0.6 kJ/mol. Thus, the results of the parametrization are certainly acceptable for these characteristics. Note that the previous covEPE parametrization scheme failed to reproduce the Si1−O* energy curve without a short-range FF correction term.[6]

While optimizing the parameters of the border centers O* and Si^{PP}*, we fixed the bond length between them in the system $(HO)_3Si-O*-Si^{PP}$* to be trained at the equilibrium distance of the reference cluster. If one used the optimized parameters for these centers and the FF parameters for the O*−Si^{PP}* interaction, then the potential energy curve of the O*−Si^{PP}* bond would fail to reproduce the reference curve; this is not really a surprise, given the purpose of these pseudopotentials. Therefore, we adjusted this interaction with a pair potential of Buckingham type, similarly to the Si(QM)−O* and O*−Si(MM) correction terms of the previous covEPE scheme.[6,19]

To assess the quality of hybrid QM/MM calculations, we optimized the structure of the $(HO)_3Si-O*-Si^{PP}$* moiety

Table 1. Characteristic Quantities Used in the Parameter Fitting of the Extended Border Scheme (New) and Corresponding Values Obtained with the Original, Simpler Scheme (Old)

		2T cluster [a]	new	Δ[b]	old	Δ[b]
PDC,[c] *e*	O*	−0.44	−0.49	−0.05	−0.38	0.06
	Si1	1.07	1.09	0.02	1.04	−0.03
	O1	−0.74	−0.72	0.02	−0.73	0.01
	O2	−0.67	−0.67	0.00	−0.68	−0.01
HOMO−LUMO, eV		6.313	6.286	−0.027	6.368	0.055
O*−Si^{PP}*, Å		1.6350	1.6351	0.0001		
O*−Si1, Å		1.6350	1.6382	0.0032		
Si1−O1, Å		1.6488	1.6523	0.0035		
O*−Si1−O1, deg		102.63	102.64	0.01		

[a] Values of the target system, see text. For the notation of the centers, see Figure 2a. [b] Deviations from the target values. [c] Potential derived charge.

and in addition compared the resulting values of the PDCs and the HOMO−LUMO gap of the trained system to those of reference 2T cluster (Table 1). The Si1−O* and Si1−O1 bonds reproduce the corresponding values of the reference cluster within 0.004 Å; the O*−Si^{PP}* bond deviates only 0.0001 Å from the reference. The O1−Si1−O* angle of the QM/MM cluster with optimum parameters and the corresponding O−Si−O angle of the reference QM system agree to 0.01°. Differences in the PDC of the trained system and the reference system deviate at most 0.02 *e* for the QM part of the hybrid system and 0.05 *e* for the border O* center. The HOMO−LUMO gap, 6.313 eV, is very well reproduced.

In Table 1, we also compare the results for PDCs and HOMO−LUMO gap obtained with the old and the new descriptions of the covEPE border. For calculations with the old approach[6] we used the same hybrid 2T cluster (Figure 2b), but the Si^{PP}* was replaced by a Si(MM) center with a positive charge of 1.182 *e* and for O* the previous parameters were used (smaller basis set, old pseudopotential parameters, compensating charge $\Delta q_{pp} = -0.282$ *e*). Both schemes reproduce yield results of similar quality. The most significant discrepancy occurs for the PDCs of the centers Si1 and O*. With the previous model, these atomic charges in the hybrid QM/MM cluster are underestimated (in absolute values) with respect to the reference cluster, while the new extended QM/MM border scheme results in a slight overestimation, closer to values used in the silica FF to model the MM environment (Si: 1.2 *e*, O: −0.6 *e*). Therefore, with the new border region, one can expect a more consistent description of the ESP both in the QM and the MM regions.

In Figure 3, we present (a) a map of the ESP calculated for a periodic array of MM point charges of chabazite structure and deviations from that target quantity for the 2T QM cluster embedded in a corresponding infinite environment of point charges using old (b) and new (c) covEPE embedding. Obviously, the new covEPE parametrization allows one to reproduce the ESP of the periodic PC array more closely than the old parametrization—not only in the center of the chabazite 8T ring at about 5 Å from the QM centers but also close to the QM oxygen centers. The largest deviations occur close to the border pseudoatoms O*. Previously, in that region the ESP was 0.4 eV (or 25.0%) more positive than the ESP of the MM reference system, −1.6 eV. With the new covEPE parametrization, the ESP near O* centers is just 0.2 eV (or 12.5%) more positive (Figure 3c).

Finally, we turn to the set of FF parameters for the interaction of border atoms with atoms of the MM environment. With the previous description,[6] the characterization of O* centers (valence orbital basis set, effective core pseudopotential with a large positive point charge of 8.7 *e*) differed notably from that of MM oxygen centers (just a pair of point charges, 2.387 *e* and −2.987 *e*). To compensate for that difference and to correctly place the QM part within its MM framework, we originally had used a special pair-potential O*−Si(MM).[6] With the new scheme on the basis of an extended QM/MM border region, Si^{PP}* TIMP centers, substituting Si^{MM} of the old scheme, form an external coordination shell of the QM partition. From the MM side, these Si^{PP}* centers are treated on the same footing as the other Si centers of the MM part, e.g., carrying a charge of 1.2 *e*. Therefore, it is natural to describe the short-range interactions between these Si^{PP}* border centers and other atomic centers of the MM region with the standard parameters of the aluminosilicate FF that we had specifically derived to model the MM environment in the covEPE embedding approach.[7] Therefore, that FF was employed to describe Si^{PP}*−O(MM) pair interactions, all three-body interactions within the Si^{PP}*O$_4$ tetrahedron, including both O* and O(MM) centers as well as the three-body interactions Si^{PP}*−O(MM)−Si(MM) and Si^{PP}*−O(MM)−Si^{PP}*. Hence, in that regard, the new parametrization affords a notably simpler and more consistent description of the interactions of atomic centers at the boundary with the MM partition of the system.

3. Computational Details

The embedded cluster calculations were carried out with the covEPE scheme[6] as implemented in the parallel density functional program PARAGAUSS.[20,21] For the QM calculations, we employed the linear combination of Gaussian-type orbitals fitting-functions density functional method (LCGTO-FF-DF).[22] We used the gradient-corrected exchange-correlation functional suggested by Becke (exchange) and Perdew (correlation);[23] all calculations were performed in spin-restricted fashion. The Kohn−Sham orbitals were represented with the following Gaussian-type basis sets,

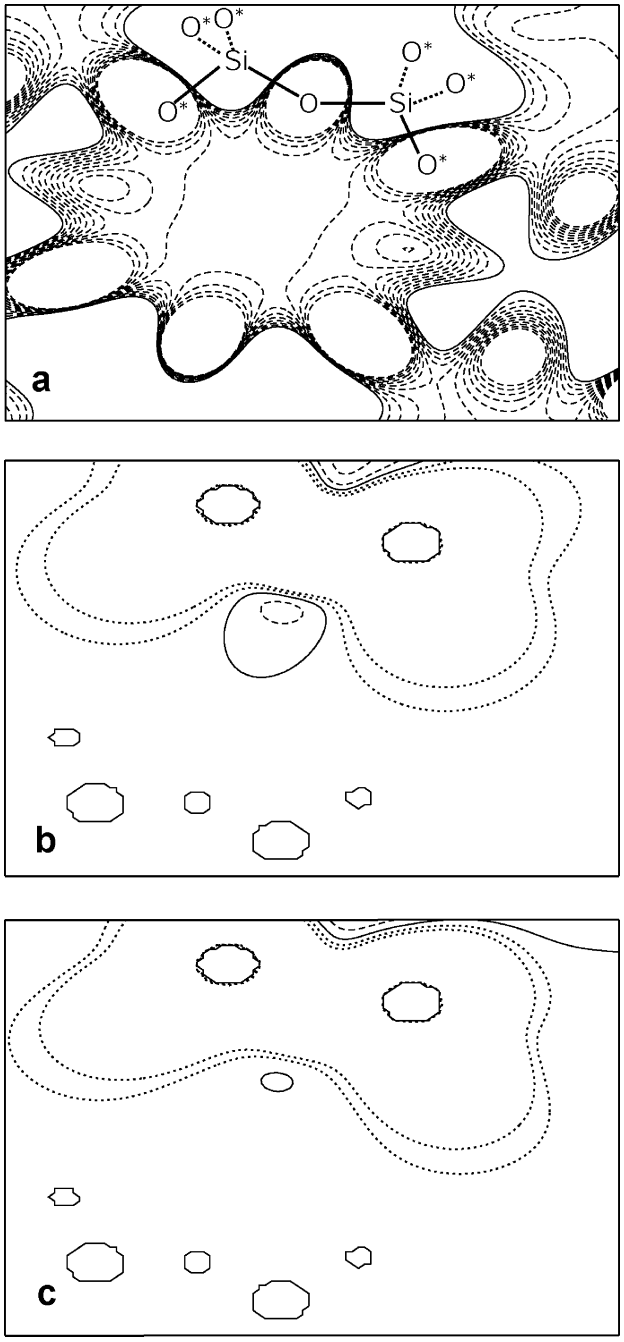

Figure 3. Electrostatic potential map calculated for a periodic array of potential-derived point charges (a) and differences between periodic ESP and ESPs calculated for a 2T QM cluster embedded in an array of point charges with (b) the old and (c) the new scheme for treating the border region. Solid, dashed, and dotted contours correspond to zero, negative, and positive ESP values, respectively; the contours represent equidistant values with an increment of 0.2 eV.

contracted in generalized fashion: (6s1p)→[4s1p] for H,[16,24] (9s5p1d)→[5s4p1d] for C and O,[16,24] and (12s9p2d)→[6s4p2d] for Al and Si.[16,24] The polarization d-exponents 0.50 and 2.05 for Si and 0.2881 and 1.0084 for Al atoms were taken from ref 25. For Rh the (19s15p10d)→[8s6p4d] basis set was constructed by adding to the (17s12p8d) basis set of Gropen[26] two s- (0.01303, 0.2253), three p- (0.03666, 0.09165, 0.2291), and two d-type exponents (0.04588, 0.1147). In the LCGTO-DF-FF method, the Hartree contribution of the electron−electron interaction is approximated by representing the electronic charge density with the help of an auxiliary Gaussian-type basis set.[22] The corresponding exponents were constructed by scaling the exponents of the orbital basis; in addition, "polarization" exponents, five each of p- and d-type, were added on each center, constructed as geometric series with a factor 2.5 starting at 0.1 au (p-exponents) or 0.2 au (d-exponents). For H centers, only p-type polarization exponents were added.

As done previously,[27,28] we applied C_3 symmetry restrictions when modeling faujasite-supported Rh_6 species to reduce the computational effort of the QM calculations (section 4.3). All other QM/MM calculations were carried out without any symmetry restrictions.

The MM part of all systems was described with the help of a FF of shell-model type[29] which we had developed for modeling silica and protonated aluminosilicates.[6,7] This force field is based on PDCs; hence, it is particularly suited for reproducing the ESP and the polarization of silica minerals and zeolite lattices.

The force constants for analyzing vibrational frequencies were calculated numerically, using finite differences of analytical energy gradients. To estimate the OH frequencies in adsorbate-free systems, we invoked the approximation of an independent harmonic oscillator, i.e., only the O−H internal coordinate was varied during the frequency calculation. Nine degrees of freedom—three for each of the centers H, C, and O (in a CO probe)—were varied during the calculations of OH and CO frequencies in the adsorption complexes of CO on zeolite OH groups.

Adsorbate−substrate binding energies, E_{ads}, were corrected for the basis set superposition error (BSSE) by applying the counterpoise method[30] in single-point fashion at the equilibrium geometry of the adsorption complexes.

4. Evaluation of the Embedding Scheme with an Extended Border Region

The quality of the new scheme for constructing an extended QM/MM border region and the corresponding parametrization of the border centers O* and Si^{PP}* were validated by calculations of structural characteristics of silicalite and alumosilicate frameworks of faujasite (FAU). In addition, we studied the OH frequencies of bridging hydroxyl groups of zeolites. Finally, we applied the new covEPE scheme to two adsorption complexes: CO probe molecules at bridging OH groups in FAU and MFI zeolites and Rh_6 clusters in the cavity of a FAU zeolite.

4.1. Silicalite of Faujasite Structure. As first check of the new parametrization of O* and Si^{PP}* centers (pseudopotentials, basis sets, correction term in the FF), we optimized the structures of QM clusters embedded in a faujasite framework containing only Si as T atoms (silicalite). The accuracy of the new scheme was evaluated from bond lengths and angles inside the embedded QM clusters and at the QM/MM border. For this comparison we used a series of five embedded QM clusters of increasing size, with two (2T) to six silicon centers (6T, Figure 4). Each QM cluster

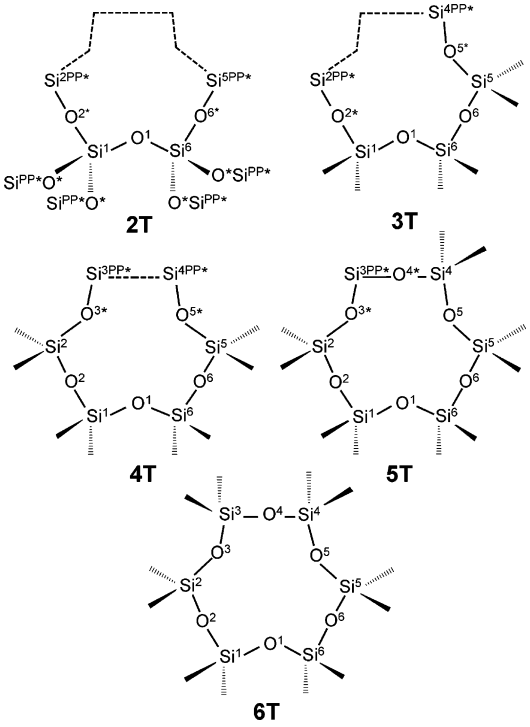

Figure 4. Pure silica QM clusters representing parts of a faujasite six-ring. The parts of the ring not included in the QM cluster are shown with dashed lines.

includes its smaller predecessors; this allows us to trace changes of structural parameters of the six-ring upon expansion of the region described at the QM level.

Inspection of Table 2 shows that structural parameters inside the QM region hardly deviate among the various models. Individual Si−O bond lengths are stable within 0.004 Å, O−Si−O angles within 1°, and Si−O−Si angles within 2°. With increasing cluster size, these structural parameters converge to the values of the largest 6T model in which a whole FAU six-ring is treated at QM level. Our calculations on the 6T model suggest that the crystallographically different oxygen centers O2 and O4 exhibit different properties in an all-silica FAU framework (Table 2, Figure 4): (i) for O2 centers, Si−O distances are 1.636 ± 0.002 Å and Si−O−Si angles are 150 ± 1° and (ii) for O4 centers, Si−O distances are 1.643 ± 0.001 Å and Si−O−Si angles are 136 ± 1°.

As our calculations do not impose structural restrictions, these differences should not be artifacts of the computational method but reflect features of the faujasite structure.

We observed slightly larger deviations, up to 0.01 Å for Si−O bonds and 4° for Si−O−Si angles, when comparing the structure of identical fragments of the FAU six-ring in different models 2T to 6T, that are treated at different computational levels, i.e., QM vs MM. Such larger deviations concern bonds and angles involving the O4 centers O^2, O^4, and O^6 which are oriented outside the six-ring. As just noted, Si−O distances of such centers are 1.643 ± 0.001 Å in the 6T model, while the same bonds described as Si(QM)−O* and O*−Si^{PP}* interactions at the border of the clusters 2T to 5T are parametrized to reproduce distances of 1.635 Å, very close to the Si−O bond lengths for O^1, O^3, and O^5 atoms in the six-ring of the 6T model. Tetrahedral O−Si−O* and O−Si−O bond angles deviate within 2° only.

The observed fluctuations of the structural parameters within the series of QM clusters, as obtained with the new covEPE description featuring an extended border region, are similar to those determined from our previous QM/MM scheme with a minimum basis set on O* border centers; calculated structure parameters, available only for 4T and 5T models,[6] agree within 0.01 Å and 3°.

4.2. Aluminosilicates. As a second test of the new method and the parametrization, we considered an aluminosilicate framework of the FAU structure with a Si/Al ratio of 47, a model system for which results are available with the previous border scheme.[7] We used 5T and 8T QM clusters with an OH group located at the O1 crystallographic position[31] and determined not only the structure of the embedded zeolite clusters but also OH frequencies and deprotonation energies (DE) of the bridging hydroxyl groups Al−O(H)−Si.

The average Al−Si distance in the 8T cluster embedded in the FAU lattice, 3.18 Å, optimized with the new scheme, is 0.03 Å shorter than the corresponding distance in the model optimized with the previous border scheme. In the same cluster the novel approach also yields shorter Al−O_b (by 0.04 Å) and Si−O_b bonds (by 0.015 Å), which agree better with recent EXAFS results.[32] In particular, with the new approach the distance Al−O_b, 1.915 Å, is quite close to corresponding experimental values, 1.89 ± 0.025 Å[32a] and 1.87 ± 0.01 Å;[32b] with the previous covEPE scheme, that distance was calculated notably longer, 1.954 Å.[7]

The observed structural changes around Al−O(H)−Si sites to some extent affect other properties of OH groups (Table 3). The OH frequency of the 8T FAU model, calculated with the extended border scheme, is 6 cm^{-1} lower than in the old approach; this result is in line with the elongation of the O_b−H bond by 0.001 Å in the new model. The deprotonation energy of faujasite in the novel scheme is reduced by 59 and 38 kJ/mol for the 5T and 8T QM clusters, respectively. The larger DE values of bridging OH groups, estimated in the previous approach, can be rationalized by a stabilization of the (neutral) initial-state structure which is caused by an artificial saturation of the small basis set of border O* centers with H basis functions of the hydroxyl group and the more positive ESP values around the border centers (see above).[7] The first factor is more pronounced in the smaller 5T QM model where the closest distance H−O* is 2.62 Å. The corresponding distance in the structure optimized with the novel border scheme is 0.11 Å longer, whereas the distance H−O_{Al} between the proton and the basic oxygen centers O_{Al} bound to Al is calculated 0.1−0.2 Å shorter (Table 3).

In summary, the novel scheme for representing the border region adequately describes the local structure of zeolites and the properties of acidic Al−O(H)−Si sites, notably improved compared to the previous border scheme of the covEPE approach.[6,7,12]

4.3. Adsorption of CO. To check the new QM/MM border scheme for interactions of guest species with a zeolite framework, we modeled the adsorption of carbon monoxide on Brønsted acidic Al−O(H)−Si centers of zeolites with

Table 2. Calculated Structural Parameters[a] of Various Silica QM Clusters, Embedded in a Faujasite Lattice, and Their Border: Bond Lengths (Å) and Bond Angles (deg)

	Si^3-O^3	O^3-Si^2	Si^2-O^2	O^2-Si^1	Si^1-O^1	O^1-Si^6	Si^6-O^6	O^6-Si^5	Si^5-O^5	O^5-Si^4	Si^4-O^4	O^4-Si^3
MM[b]	1.632	1.632	1.626	1.626	1.632	1.632	1.626	1.626	1.632	1.632	1.626	1.626
2T			1.634[d]	1.634[c]	1.639	1.640	1.636[c]	1.635[d]				
3T			1.634[d]	1.638[c]	1.638	1.638	1.644	1.644	1.635[c]	1.631[d]		
4T	1.631[d]	1.634[c]	1.643	1.643	1.636	1.637	1.645	1.644	1.634[c]	1.631[d]		
5T	1.632[d]	1.637[c]	1.647	1.642	1.636	1.637	1.644	1.642	1.637	1.636	1.637[c]	1.633[d]
6T	1.634	1.636	1.643	1.642	1.635	1.636	1.644	1.642	1.637	1.636	1.643	1.643
Δ[e]	0.003	0.002	0.009	0.008	0.004	0.004	0.008	0.007	0.003	0.005	0.006	0.010

	$Si^3-O^3-Si^2$	$Si^2-O^2-Si^1$	$Si^1-O^1-Si^6$	$Si^6-O^6-Si^5$	$Si^5-O^5-Si^4$	$Si^4-O^4-Si^3$
MM[b]	146	148	146	148	146	148
2T		140[c]	147	139[c]		
3T		139[c]	148	135	152[c]	
4T	151[c]	135	148	135	153[c]	142[f]
5T	151[c]	135	149	135	149	140[c]
6T	150	136	149	135	150	136
Δ[e]	1	4	2	4	3	4

	$O^4-Si^3-O^3$	$O^3-Si^2-O^2$	$O^2-Si^1-O^1$	$O^1-Si^6-O^6$	$O^6-Si^5-O^5$	$O^5-Si^4-O^4$
MM[b]	107	107	107	107	107	107
2T		108[d]	107	107	108[d]	
3T	108[d]	108[c]	107	108	110	110[d]
4T	109[d]	109	108	108	110	110[d]
5T	109[c]	109	108	108	109	108[c]
6T	109	108	108	108	109	109
Δ[e]	0	1	1	1	2	2

[a] For the notations of the models and various centers, see Figure 4. [b] Values of an infinite FAU lattice, described by the force field. [c] Si(QM)−O* and Si(QM)−O*−Si^{PP}* at the QM/MM border. [d] O*−Si^{PP}* and O*−Si^{PP}*−O(MM) at the QM/MM border. [e] Maximum deviation of QM results from the corresponding values of the largest QM model, 6T. [f] Si^{PP}*−O(MM)−Si^{PP}* at the QM/MM border.

Table 3. Selected Structural Parameters (in Å and deg), Harmonic OH Frequencies ν(OH) (in cm^{-1}), and Deprotonation Energies DE (in kJ/mol) for Acidic Al−O_b(H)−Si Sites from 5T and 8T QM Models Embedded in a Faujasite Lattice (Si/Al = 47) with Bridging Oxygen Centers O_b Located at O1 Crystallographic Positions

	previous border scheme[a]			extended border scheme[b]		
QM cluster	5T	8T	Δ[c]	5T	8T	Δ[c]
Al−O_b	1.958	1.954	−0.004	1.929	1.915	−0.014
<Al−O>[d]	1.721	1.722		1.719	1.720	
Si−O_b	1.718	1.722	0.004	1.707	1.707	0.000
<Al−Si>[d]	3.21	3.21		3.18	3.18	
O_b−H	0.976	0.978	0.002	0.979	0.979	0.000
H−O*[e]	2.618	4.569		2.729	4.591	
H−O_{Al}[f]	2.80	2.70		2.59	2.61	
Al−O_b−Si	128.7	131.3	2.6	128.7	129.9	1.2
H−O_b−Al	114.0	111.2	−2.8	112.2	112.8	0.6
H−O_b−Si	117.1	115.8	−1.3	119.1	117.2	−1.9
ν(OH)	3754	3720	−34	3683	3714	31
DE	1285	1270	−15	1226	1232	6

[a] Reference 7. [b] Present work. [c] Changes in the results of the 8T QM model with respect to the results of the 5T QM model. [d] Average value. [e] Distance between the acidic H and the nearest pseudoatom O*. [f] Distance between the acidic H and the oxygen connected to the Al atom.

FAU and MFI structures as this molecule is often used as a probe for the acidity of zeolite OH groups.[33] This interaction is characterized with a relatively small adsorption energy,[34−37] and thus, minor inaccuracies in the description of the boundary region can be crucial, in particular for small embedded QM models. For FAU we modeled the interaction of CO with hydroxyl groups at O1 crystallographic positions, using a 8T QM cluster (Figure 5a). For HZSM-5 zeolite, the probe was assumed to adsorb at the Al7−O17(H)−Si4 site, modeled by a 9T QM cluster (Figure 5b).

In Table 4, we have collected calculated structural parameters, the adsorption energy of CO, E_{ads}, and shifts of the vibrational frequencies C−O and O−H, obtained with the original and the extended border schemes.

The adsorption energy of CO, corrected for the BSSE, determined with the novel scheme of the border region, is 18.6 kJ/mol, both in faujasite and HZSM-5. This value is close to the BSSE corrected adsorption energy of CO in chabazite, 16.0 kJ/mol, obtained in periodic B3LYP calculations.[37] With the previous border scheme, where a small basis set was used for O* centers, the uncorrected E_{ads} values were 28.8 kJ/mol for FAU and 44.8 kJ/mol for MFI, but only 11−12 kJ/mol remained after correction for the BSSE. Thus, 60−75% of these values were caused by basis functions of the adsorbate saturating the small O* basis set. With the novel border scheme, the fraction of the BSSE is considerably reduced, to 25%.

The geometry optimized with the novel approach suggests that CO molecules are almost linearly orientated relative to the hydroxyl group; the H−C−O angle is calculated at 173° in FAU and 176° in MFI. These values agree well with the

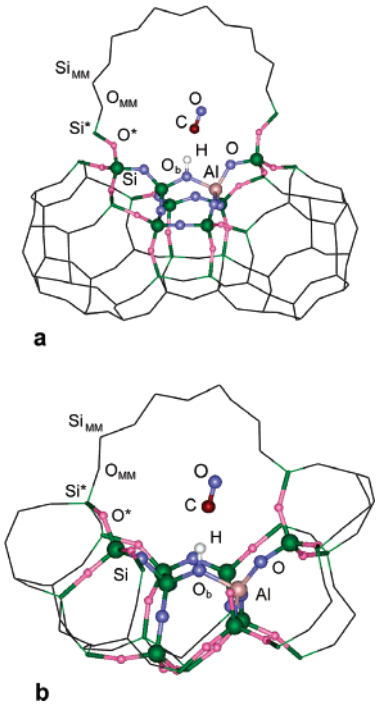

Figure 5. Optimized structures of models of CO adsorption on zeolite QM clusters embedded in lattices of (a) FAU and (b) MFI structure.

corresponding result, 176°, determined in a periodic B3LYP supercell calculation for CO adsorption in chabazite.[37] Our calculated distances, OC···H 1.90 Å for FAU, and 1.94 Å for MFI, are also close to the B3LYP result, 1.95 Å.[37] CO adsorption on acidic sites is accompanied by an elongation of the O−H bond, by 0.025 Å for FAU and 0.022 Å for MFI, while the C−O bond is contracted by 0.004 Å in both zeolite structures. These changes in bond lengths agree with calculated (Table 4) and experimentally observed[33] trends for the changes of the vibrational frequency shifts, a strong red shift of the OH band and a smaller blue shift of the CO frequency.

Our prediction of an elongated O−H bond and a related reduction of the O−H frequency upon adsorption of a CO probe on Al−O(H)−Si sites is in line with results of experimental[33] and previous theoretical studies.[34−37] However, the red shifts of the OH frequency, calculated at 425 cm^{-1} for MFI and 500 cm^{-1} for FAU (Table 4), are larger than the measured bathochromic shifts of the OH band, 307−320 cm^{-1} for MFI and 295−353 cm^{-1} for FAU.[33] This underestimation of the OH vibrational frequency of adsorption complexes of CO on OH groups can be considered as a feature of the density functional method used. For example, a large OH red shift of 375 cm^{-1} was recently reported from periodic B3LYP calculations on H-chabazite (Si/Al = 11).[37,38]

IR measurements predict an increase of the CO frequency by 32 ± 2 cm^{-1} after adsorption of CO probes at zeolite Brønsted sites, both for HZSM-5 and FAU.[33,37] With the extended border scheme, we calculated C−O red shifts of 37 cm^{-1} and 42 cm^{-1}, for CO adsorption on acidic OH group of zeolites with FAU and MFI structure, respectively, in good agreement with the IR data. However, the previous scheme

Table 4. Selected Structural Parameters (in Å and deg), Frequency Shifts $\Delta\nu$(OH) and $\Delta\nu$(CO) (in cm^{-1}) of the OH and CO Vibrational Modes, Respectively, Adsorption Energy E_{ads} of CO Corrected for the Basis Set Superposition Error (BSSE) and BSSE Correction (in kJ/mol) of CO Complexes on Zeolites of FAU and MFI Structure[a]

	previous border scheme		extended border scheme	
	FAU	MFI	FAU	MFI
O_b−H	1.001	0.999	1.004	0.998
C−O	1.143	1.147	1.141	1.141
OC···H	1.919	1.970	1.896	1.941
O_b−H−C	158.7	167.3	168.3	170.9
H−C−O	174.1	150.9	172.9	175.7
C···O*	3.29	2.49	3.82	3.15
O···O*	2.92	2.88	3.65	3.14
C···Si(MM)	4.51	3.31	4.99	3.91
C···O(MM)	4.58	3.13	4.87	3.34
O···Si(MM)	3.82	3.01	4.52	3.43
O···O(MM)	3.60	2.29	4.07	2.46
Δr(O−H)[b]	0.023	0.022	0.025	0.022
$\Delta\nu$ (OH)[c]	−459	−335	−502	−425
Δr(C−O)[d]	−0.002	+0.002	−0.004	−0.004
$\Delta\nu$(CO)[e]	31	−13	37	+42
E_{ads}	11.6	11.1	18.6	18.6
BSSE	17.2	33.7	5.9	6.7

[a] For the structure of the complexes and the notation of the centers, see Figure 5. [b] Change of the O−H distance with respect to an adsorbate-free zeolite. [c] Frequency shift with respect to ν(OH) in an adsorbate-free zeolite. [d] Change of the C−O distance with respect to a free CO molecule. [e] Frequency shift with respect to ν(CO) of a free CO molecule, 2091 cm^{-1}.

for the QM/MM border region was less successful in describing CO adsorption at the OH groups; the interaction of CO molecules with the nearest border O* center was overestimated. This effect is particularly important for zeolites with narrower pores, e.g., MFI with 10-member ring of 5.5 Å diameter, where C and O centers of the adsorbate are located only 2.49 and 2.88 Å, respectively, from the nearest O* center (Table 4). As a consequence of this artificial interaction, adsorption complexes of CO species were notably bent, with an H−C−O angle of only 151°. A further consequence is an elongation of the C−O distance in adsorbed CO, by 0.002 Å compared to a free CO molecule, and a corresponding *reduction* of the C−O vibrational frequency upon adsorption (Table 4), i.e. the CO frequency was calculated to shift in the direction opposite to experiment. In the FAU model, adsorption complexes of CO at OH groups are less affected by border O* centers, because the cavity of this structure is wider (12-member ring, 12 Å diameter) and the active site is farther from the border O* centers. However, even in the FAU model, the C···O* and O···O* distances were calculated about 0.6 Å shorter with the previous approach than with the present extended border scheme.

Thus, with the improved scheme for constructing the boundary region, one is able to predict structural, spectroscopic, and energetic characteristics of CO adsorption at acidic OH groups of zeolites in good agreement with

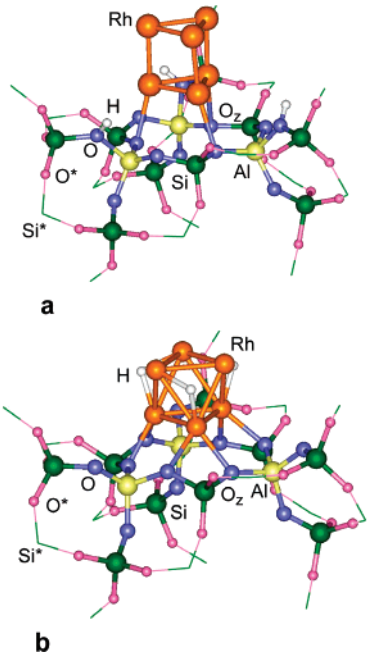

Figure 6. Optimized structures of the 12T QM embedded models representing adsorption complexes of (a) bare Rh_6 and (b) hydrogen-containing Rh_6H_3 clusters on a faujasite six-ring.

available experimental and calculated data, thus avoiding artifacts that occurred with the previous, simpler QM/MM border approach.

4.4. Adsorption of Rh_6 Metal Cluster. Finally, we turn to an important benchmark system where bulky metal particles are adsorbed in zeolite cavities. Previously, we described Rh_6 in FAU with isolated cluster models of the zeolite support[27,39] to clarify earlier EXAFS studies.[40] With finite six-ring models of zeolite, we studied two forms of supported Rh_6 clusters: bare Rh_6, denoted as Rh_6/zeo(3H), and hydrogen-covered Rh_6H_3, denoted as Rh_6(3H)/zeo. The latter species, formally obtained by transfer of three protons from bridging OH groups of the zeolite to the metal cluster ("reverse hydrogen spillover"), were calculated to be preferred for a large variety of late transition metals, including Rh.[28] In the present context, we modeled both species (Figure 6) with either of the two border schemes (Table 5). For the Rh_6/zeo(3H) structure (Figure 6a) we considered bridging OH groups at O1 crystallographic positions of hexagonal prisms of the FAU structure, i.e., close to zeolite six-rings (Figure 6a).

With the new, extended border scheme, the BSSE-corrected adsorption energy, E_{ads}, of Rh_6 in Rh_6/zeo(3H) was calculated at 64 kJ/mol (Table 5). This value is by only 9 kJ/mol lower than $E_{ads} = 73$ kJ/mol, calculated with the finite model.[27] With the previous QM/MM border scheme, the BSSE-corrected value, $E_{ads} = 31$ kJ/mol, was underestimated as a consequence of a large BSSE, 399 kJ/mol. The main contribution to BSSE originates from saturating the basis set of the zeolite fragment (in particular, of O* centers with a small basis set) by the basis set of the adsorbate. With the extended border scheme, the BSSE is very significantly reduced, to only 39 kJ/mol, but the main contribution (79%) again is due to complementing the zeolite basis set.

Table 5. Selected Interatomic Distances (in Å) in Faujasite-Supported Bare Rh_6 and Hydrogen-Covered Rh_6H_3 Clusters,[a] Energies E_{ads} of Adsorption of the Cluster Rh_6 on the Zeolite Support, Corrected for the Basis Set Superposition Error (BSSE), BSSE Values, and Energies E_{RS} of Reverse Proton Spillover onto the Supported Metal Clusters (in kJ/mol)

	previous border scheme		extended border scheme	
	Rh_6/zeo(3H)	Rh_6(3H)/zeo	Rh_6/zeo(3H)	Rh_6(3H)/zeo
Rh−Rh[b]	2.45−2.57	2.60−2.64	2.47−2.51	2.57−2.65
Rh−H		1.72; 1.77		1.72; 1.78
Rh−O_z[c]	2.29	2.14; 2.18	2.49	2.16; 2.21
Rh−O*[d]	3.01	3.34	3.28	3.35
E_{ads}	31		64	
BSSE	410		39	
E_{RS}	237		240	

[a] See Figure 6. [b] Experimental value 2.67−2.69 Å, ref 40. [c] Distance between nearest neighbors Rh and oxygen centers O_z of the zeolite support; experimental values: 2.10−2.17 Å, ref 40. [d] Distance between nearest neighbors Rh and O* centers.

In contrast to the strong influence on the adsorption energy of the Rh_6 cluster in Rh_6/zeo(3H), the border scheme has essentially no effect on the energy, E_{RS}, of reverse hydrogen spillover. It was calculated at 240 kJ/mol in the new scheme and 237 kJ/mol in the previous border scheme (Table 5). This can be rationalized by the fact that in this case one compares two structural isomers, Rh_6/zeo(3H) and Rh_6(3H)/zeo. Therefore, the influence of the BSSE on E_{RS} is, to a very large extent, eliminated as we are using the same basis sets when calculating the (formal) initial and final states of reverse spillover. With respect to isolated cluster calculations,[39] the energy E_{RS} is reduced by about 35%.

The calculations with both border schemes suggest that the bare adsorbed Rh_6 cluster is farther from its support and concomitantly features shorter Rh−Rh nearest-neighbor distances than the hydrogenated cluster Rh_6H_3, similarly to the results from the isolated cluster models.[27,39] In the previous border scheme, the artificial attraction between the adsorbate and the O* centers reduces the Rh−O* distance in the structure Rh_6/zeo(3H) by 0.27 Å compared to the structure optimized with the new approach. In addition, the Rh−O_z distance between the rhodium atoms at the "bottom" triangle of the Rh_6 species and the oxygen atoms of the zeolite six-ring increases notably, from 2.29 Å to 2.49 Å, when one switches from the previous to the new border schemes. The metal−metal distances in the Rh_6/zeo(3H) structure change much less between the two embedding schemes, at most 0.06 Å (Table 5).

Likely, due to the large Rh−O* separation, 3.35 Å, in the hydrogenated Rh_6(3H)/zeo complex, this structure remains essentially unaffected by the improved description of the border region. The distances Rh−O_z, Rh−Rh, and Rh−H of the two models agree within 0.03 Å, 0.03 Å, and 0.01 Å, respectively.

In a recent paper, we discussed in detail interatomic distances in the structures of the supported clusters, optimized

with the novel border scheme.[41] There, we showed that available EXAFS data[40] for the metal−metal distances of Rh_6 species in Y zeolites, 2.67−2.69 Å, and distances between metal and oxygen centers of the support, 2.10−2.17 Å, are consistent with Rh−Rh (2.57−2.65 Å) and Rh−O_z distances (2.14−2.21 Å), calculated for the hydrogenated Rh_6(3H)/zeo model, while the corresponding values for the bare cluster Rh_6/zeo(3H) differ by about 0.2 Å. The same conclusion was drawn from results obtained with finite models of the zeolite support.[27,41]

5. Conclusions

The present work reported an improved scheme for constructing the border region within a hybrid embedded cluster approach covEPE for zeolites and covalent oxides. The new scheme assures proper modeling of adsorbates interacting with such types of support.[6,7] At variance with the original implementation of the covEPE method, where monovalent O* pseudoatoms at the QM border were described with a small basis set, the basis set on those centers in the present, an improved scheme is as flexible as that normally used for O centers of the QM cluster. These new O* centers are much more polarizable due to their large basis set. To avoid polarization artifacts, we extended the border region by a second "layer" of border centers, at Si centers of the MM region that are immediate neighbors of the QM O* centers. Both, O* and Si^{PP}* centers were modeled as pseudopotentials. The parameters of both types of pseudopotentials and the basis set of O* centers were optimized by targeting structural and electronic properties of model zeolite fragments.

The resulting improved hybrid QM/MM scheme affords a correct description of the local structure of silica and aluminosilicate zeolites and of the properties of bridging OH groups. These properties are reproduced at notably improved quality compared to results of covEPE models that were constructed with the previous border scheme.[7]

With the novel border scheme, we achieved good agreement with available experimental and reliable computational data for the adsorption of CO probe molecule on bridging OH groups of zeolites with MFI and FAU structures. Changes induced upon CO adsorption in the structure of zeolite acidic OH sites, the CO vibrational frequency shift, and the adsorption energy of CO, calculated with an 8T embedded QM cluster, are considerably improved as compared to analogous results obtained with the previous border scheme using a small basis set on the capping O* centers. The good performance of the new approach is accompanied with a substantial reduction of the BSSE, which in the previous construction of the border region originated from an implicit augmentation of the small basis set of the O* centers by basis functions of the adsorbates.

Models with the new border scheme are also well suited to describing large adsorbates, e.g., transition-metal clusters, with satisfactory accuracy. Here, too, the new scheme exhibits greatly reduced BSSE corrections compared to the previous method for constructing border O* centers. Recently, we successfully applied the new border scheme to calculate the energetics of reverse hydrogen spillover from zeolite hydroxyl groups to supported Ir_6 clusters and the lack of such spillover in the case of Au_6 clusters.[41]

Acknowledgment. E.A.I.S. gratefully acknowledges an individual grant of the Krasnoyarsk Regional Scientific Foundation (grant 15G127). This work was supported by Volkswagen-Stiftung (grant I/73653), Deutsche Forschungsgemeinschaft, Fonds der Chemischen Industrie, Bulgarian National Science Fund, and an integration project (no. 79) of the Siberian Branch of the Russian Academy of Sciences.

Supporting Information Available: Tables with the optimized parameters of the border centers and a figure with potential energy curves calculated for the reference 2T cluster and the trained system on the basis of the optimized parameters. This material is available free of charge via the Internet at http://pubs.acs.org.

References

(1) (a) Sherwood, P.; de Vries, A. H.; Guest, M. F.; Schreckenbach, G.; Catlow, C. R. A.; French, S. A.; Sokol, A. A.; Bromley, S. T.; Thiel, W.; Turner, A. J.; Billeter, S.; Terstegen, F.; Thiel, S.; Kendrich, J.; Rogers, S. C.; Casci, J.; Watson, M.; King, F.; Karlsen, E.; Sjøvoll, M.; Fahmi, A.; Schäfer, A.; Lennartz, C. *J. Mol. Struct. Theochem* **2003**, *632*, 1−28. (b) Sauer, J.; Sierka, M. *J. Comput. Chem.* **2000**, *21*, 1470−1493.

(2) (a) Sherwood, P. In *Modern Methods and Algorithms of Quantum Chemistry*, *NIC Series Volume 1*; J. von Neumann Institute for Computing: Julich, 2000; pp 301−449. (b) Sokol, A. A.; Bromley, S. T.; French, S. A.; Catlow, C. R. A.; Sherwood, P. *Int. J. Quantum Chem.* **2004**, *99*, 695−712.

(3) (a) Nasluzov, V. A.; Rivanenkov, V. V.; Gordienko, A. B.; Neyman, K. M.; Birkenheuer, U.; Rösch, N. *J. Chem. Phys.* **2001**, *115*, 8157−8171. (b) Rösch, N.; Nasluzov, V. A.; Neyman, K. M.; Pacchioni, G.; Vayssilov, G. N. In *Computational Material Science*; Theoretical and Computational Chemistry Series, Leszczynski, J., Ed.; Elsevier: Amsterdam, 2004; Vol. 15, pp 365−448.

(4) Vreven, T.; Morokuma, K. *J. Comput. Chem.* **2000**, *21*, 1419−1432.

(5) (a) Gao, J. L.; Amara, P.; Alhambra, C.; Field, M. J. *J. Phys. Chem. A* **1998**, *102*, 4714−4721. (b) Antes, I.; Thiel, W. *J. Phys. Chem. A* **1999**, *103*, 9290−9295.

(6) Nasluzov, V. A.; Ivanova, E. A.; Shor, A. M.; Vayssilov, G. N.; Birkenheuer, U.; Rösch, N. *J. Phys. Chem. B* **2003**, *107*, 2228−2241.

(7) Ivanova Shor, E. A.; Shor, A. M.; Nasluzov, V. A.; Vayssilov, G. N.; Rösch, N. *J. Chem. Theory Comput.* **2005**, *1*, 459−471.

(8) Sulimov, V. B.; Sushko, P. V.; Edwards, A. H.; Shluger, A. L.; Stoneham, A. M. *Phys. Rev. B* **2002**, *66*, 024108.

(9) Mukhopadhyay, S.; Sushko, P. V.; Stoneham, A. M.; Shluger, A. L. *Phys. Rev. B* **2005**, *71*, 235204.

(10) (a) Joshi, Y. V.; Thomson, K. T. *J. Catal.* **2005**, *230*, 440−463. (b) To, J.; Sherwood, P. Sokol, A. A.; Bush, I. J.; Catlow, C. R. A.; van Dam, H. J. J.; French, S. A.; Guest, M. F. *J. Mater. Chem.* **2006**, *16*, 1919−1926.

(11) Tuma, C.; Sauer, J. *Chem. Phys. Lett.* **2004**, *387*, 388−394.

(12) Deka, R. C.; Ivanova Shor, E. A.; Shor, A. M.; Nasluzov, V. A.; Vayssilov, G. N.; Rösch, N. *J. Phys. Chem. B* **2005**, *109*, 24304−24310.

(13) Dolg, M.; Wedig, U.; Stoll, H.; Preuss, H. *J. Chem. Phys.* **1987**, *86*, 866−872.

(14) Bergner, A.; Dolg, M.; Küchle, W.; Stoll, H.; Preuss, H. *Mol. Phys.* **1993**, *80*, 1431−1441.

(15) Stevens, W. J.; Basch, H.; Krauss, M. *J. Chem. Phys.* **1984**, *81*, 6026−6033.

(16) Van Duijnevelt, F. B. *IBM Research report No. RJ*; 1971; p 945.

(17) Fuentealba, P.; Preuss, H.; Stoll, H.; von Szentpály, L. *Chem. Phys. Lett.* **1982**, *89*, 418−422.

(18) Nelder, J. A.; Mead, R. *Comput. J.* **1965**, *7*, 308−313.

(19) The parameters for the correction Buckingham type pair-potential for the O*−Si^{PP}* interaction are 31156.5 eV (A), 0.199145 Å (ρ), and 237.804 eV·Å^6 (C).

(20) Belling, T.; Grauschopf, T.; Krüger, S.; Nörtemann, F.; Staufer, M.; Mayer, M.; Nasluzov, V. A.; Birkenheuer, U.; Hu, A.; Matveev, A. V.; Shor, A. M.; Fuchs-Rohr, M. S. K.; Neyman, K. M.; Ganyushin, D. I.; Kerdcharoen, T.; Woiterski, A.; Gordienko, A. B.; Majumder, S.; Rösch, N. *ParaGauss version 3.0*; Technische Universität München: Garching, Germany, 2004.

(21) Belling, T.; Grauschopf, T.; Krüger, S.; Mayer, M.; Nörtemann, F.; Staufer, M.; Zenger, C.; Rösch, N. In *High Performance Scientific and Engineering Computing*; Lecture Notes in Computational Science and Engineering, Bungartz, H.-J., Durst, F., Zenger, C., Eds.; Springer: Heidelberg, 1999; Vol. 8, pp 441−455.

(22) Dunlap, B. I.; Rösch, N. *Adv. Quantum Chem.* **1990**, *21*, 317−339.

(23) (a) Becke, A. D. *Phys. Rev. A* **1988**, *38*, 3098−3100. (b) Perdew, J. P. *Phys. Rev. B* **1986**, *33*, 8822−8824; **1986**, *34*, 7406.

(24) (a) *Gaussian Basis Sets for Molecular Calculations*; Huzinaga, S., Ed.; Elsevier: Amsterdam, 1984. (b) Veillard, A. *Theor. Chim. Acta* **1968**, *12*, 405−411.

(25) Bär, M. R.; Sauer, J. *Chem. Phys. Lett.* **1994**, *226*, 405−412.

(26) Gropen, O. *J. Comput. Chem.* **1987**, *8*, 982−1003.

(27) Vayssilov, G. N.; Gates, B. C.; Rösch, N. *Angew. Chem., Int. Ed.* **2003**, *42*, 1391−1394.

(28) Vayssilov, G. N.; Rösch, N. *Phys. Chem. Chem. Phys.* **2005**, *7*, 4019−4026.

(29) Dick, B. G.; Overhauser, A. W. *Phys. Rev. B* **1958**, *112*, 90−103.

(30) Boys, S. F.; Bernardi, F. *Mol. Phys.* **1970**, *19*, 553−566.

(31) The structures of the QM model clusters are shown in Figure 2a,b of ref 7.

(32) van Bokhoven, J. A.; van der Eerden, A. M. J.; Prins R. *J. Am. Chem. Soc.* **2004**, *126*, 4506−4507. (b) Joyner, R. W.; Smith, A. D.; Stockenhuber, M.; van den Berg, M. W. E. *Phys. Chem. Chem. Phys.* **2004**, *6*, 5435−5439.

(33) Hadjiivanov, K. I.; Vayssilov, G. N. *Adv. Catal.* **2002**, *47*, 307−511.

(34) Strodel, P.; Neyman, K. M.; Knözinger, H.; Rösch, N. *Chem. Phys. Lett.* **1995**, *240*, 547−552.

(35) Senchenya, I. N.; Garrone, E.; Ugliengo, P. *J. Mol. Struct. Theochem* **1996**, *368*, 93−110.

(36) Brand, H. V.; Redondo, A.; Hay, P. J. *J. Mol. Catal. A* **1997**, *121*, 45−62.

(37) Ugliengo, P.; Busco, C.; Civalleri, B.; Zicovich-Wilson, C. M. *Mol. Phys.* **2005**, *103*, 2559−2571.

(38) The vibrational shift seems to increase with the size of the basis set on hydrogen. For example, addition of a p-type polarization exponent to the basis set of hydrogen increases the shift of the OH frequency, from 300 cm^{-1} to 344 cm^{-1}, in BLYP calculations of CO adsorption at the 2T cluster model $H_3Al-O(H)-SiH_3$.[36] Therefore, results from a more flexible basis set should not necessarily be expected to agree better with experiment.

(39) Vayssilov, G. N.; Rösch, N. *J. Phys. Chem. B* **2004**, *108*, 180−197.

(40) Weber, W. A.; Gates, B. C. *J. Phys. Chem. B* **1997**, *101*, 10423−10434.

(41) Ivanova Shor, E. A.; Nasluzov, V. A.; Shor, A. M.; Vayssilov, G. N.; Rösch, N. *J. Phys. Chem. C* **2007**, *111*, 12340−12351.

CT700159K